Characterization of sensor location variations in admittance-based TPA methods

Domen Ocepek[a], Gregor Čepon[a,*], Miha Boltežar[a]

[a] *University of Ljubljana, Faculty of Mechanical Engineering, Aškerčeva 6, 1000 Ljubljana, Slovenia*

Cite as:
Domen Ocepek, Gregor Čepon, Miha Boltežar,
Characterization of sensor location variations in admittance-based TPA methods,
Journal of Sound and Vibration, 2022, https://doi.org/10.1016/j.jsv.2022.116888

Abstract

When determining the critical paths for the transmission of sound and vibration in assembly products, transfer path analysis (TPA) is a reliable and effective tool. TPA represents a source with a set of forces that replicate the operational responses. However, admittance-based TPA methods are prone to experimental errors, as small measurement inaccuracies can lead to large discrepancies in the source characterization. The admittance of the transfer paths is preferably obtained through impact testing. Thus, poor repeatability in the position of the successive impacts affects the consistency of the interface forces. In this study, uncontrolled location variations in a structure's excitation are characterized by a sensitivity analysis based solely on an experimental model. The functional dependency of a frequency response function on the impact location is deduced from the measured data. This makes it possible to reconstruct numerous responses for variations in the impact location and provides an appropriate sample size for the global sensitivity analysis. The influence of a random error at an individual impact location is quantified on the basis of variations in the response prediction. The approach is useful for cases where the source characterization is affected by location variations of the force input, e.g., lightly damped or complex structures where the impact locations are not easily accessed. An experimental study on an electric motor demonstrates that controlling the impact location's repeatability in a TPA is important and can lead to a more consistent source characterization.

Keywords: Transfer path analysis, Impact excitation, Location uncertainty, Sensitivity analysis, Cross validation, Electric motor

---

1. Introduction

Transfer path analysis (TPA) is a reliable and effective diagnostic tool for the characterization of actively vibrating components and the propagation of noise and vibration to connected passive substructures. TPA can analyse the vibration transfer between the individual components of the assembly, distinguish the partial transfer path contribution and predict the receiver's response. As such, it has gained attention as a valuable step in the product-development phase.

For the source characterization a set of forces, applied at the interfaces between the individual components, is estimated. This represents the vibrating source. Two families of TPA methods can be applied accordingly: classical and component-based TPA [1]. Classical TPA methods describe source excitations in terms of the interface forces [2]. This approach has one major drawback, as the determined forces are valid for the measured assembly only. For an independent characterization of the source structure, component-based

*Corresponding author
Email address: `gregor.cepon@fs.uni-lj.si` (Gregor Čepon)

TPA adopts a different approach. Here, a set of equivalent forces counteracts the operational excitation and thus blocks the motion downstream of the interface. These equivalent or blocked forces are valid for any assembly with a modified passive side [1, 3].

The load on the interface can be measured directly or indirectly. A direct load determination using force transducers mounted at the connection interface is difficult in practice [4]. The indirect determination of the forces at the interface in multiple degrees of freedom (DoFs) is therefore often performed using an inverse procedure. Different admittance-based TPA methods for the various boundary conditions of the active component were proposed [1], with the in-situ TPA [1, 5] even eliminating the need to dismount any part of the assembly. Combining the concepts of TPA with the principles of Dynamic Substructuring (DS) has led to an approach in which the source is characterized using forces and moments in a virtual point (VP) [6]. The virtual point, typically used in frequency based substructuring (FBS) applications [7], has the advantage of taking into account moments in the transfer paths that are otherwise not measurable with conventional force transducers [8].

Admittance-based TPA methods are often strongly influenced by imperfect measurements. Given that the condition number of the transfer path admittance is high, this can lead to a severe error amplification in the interface forces. In order to overcome this problem, regularization techniques such as singular value truncation [9, 10] or Tikhonov regularization [10, 11] are usually suggested. These techniques improve the accuracy of the determined interface forces, but do not provide information about the quality of the measurement. In general, the measurement errors can be classified according to their nature into two categories: random errors and systematic errors (also called bias). Random errors in the TPA framework can be evaluated and quantified with statistical tools [12, 13]. They affect the reliability, but not the accuracy of the outcome. Bias errors are inherent to the system and affect the accuracy of the measurement outcome. As the true value of the measured quantity is unknown, bias errors are difficult to properly quantify and correct.

Assume one measures a system's frequency response functions (FRFs) with an impulse hammer and a fixed accelerometer on the structure. Regarding the response measurement, the most prominent measurement errors are systematic errors that arise from erroneous positioning, mass loading, added stiffness and additional damping from the sensor cabling. The careful design of the experiment helps to minimize the bias errors in response measurements. However, positioning the sensors on the structure is not straightforward and is of key importance in a TPA characterization. Some practical considerations about the sensor's placement around the transfer paths and an over-determination of the inverse problem were provided in [9]. Furthermore, Wernsen et al. [9] studied pollution of the equivalent forces due to sensor noise and suggested regularization techniques to attenuate the equivalent force noise. It is also suggested to use compliant test benches with a higher signal-to-noise ratio (SNR) to minimize the effects of the sensor noise [14]. In contrast, inconsistencies in the measured structure excitations introduce a much larger problem when determining the interface forces. Usually, impact testing is preferable to the shaker setup in order to obtain the transfer path admittance due to the practical FRF acquisition at each separate impact location. Offsets of the successive impacts are thus very dependent on the experimentalist and good repeatability between impacts is challenging to achieve. It is common that the impact location varies slightly for every hit, especially if the interface region is not easily accessible. If one averages multiple FRFs, as is usually the case with impact testing, these misalignments introduce an uncertainty into the FRFs. Interface forces are thus sensitive to error amplification since the FRFs are inverted in the inverse problem. In the frequency domain, methods to identify inconsistent measurements (impacts) were already proposed using expansion techniques [15, 16]. However, this requires an equivalent numerical model of the structure, which, despite the remarkable advances in numerical simulation, might not reflect the dynamic behaviour of the actual system.

In this work, a sensitivity-based approach is proposed to characterize the influence of the random variations in impact location within the TPA, based solely on the experimental model. A mathematical model is established, describing the relation between the FRF and the location error. The formulation is based on the assumption that the FRFs at the individual force input and the omnidirectional location offset are linearly dependent for a small offset error [17, 18]. Linear dependency makes it possible to reconstruct numerous FRFs for each excitation location at arbitrary offsets, which would be practically impossible to obtain with measurements. A sizable FRF set is necessary for a meaningful sensitivity analysis (SA). A Saltelli sample scheme [19] is proposed to generate the offset locations for reconstructed FRFs and a Sobol sensitivity analysis [20, 21] to quantify how sensitive the interface forces are to a random location error for an individual excitation location. The evaluation model for the SA is based on an on-board validation, a tool typically used to estimate the source characterization's completeness [4], to assess how it varies due to input variations. The proposed methodology is demonstrated on an in-situ TPA, because of its widespread use. However, it is applicable to the arbitrary admittance-based TPA method, from both the classical and component-based families. To present the efficiency of the proposed approach, an experimental case study on a real complex structure is presented. The source characterization is performed on an electric motor. The equivalent forces are built from impacts with low sensitivity only, and evaluated using on-board and cross validation. Compared to the case with all the impacts included, an improved prediction of the passive substructure's response can be observed.

This paper is organized as follows. The following section summarizes the basic theory of an in-situ TPA and virtual point transformation (VPT). Section 3 presents the proposed approach for the characterization of random errors in the impact location within the TPA methodology. Section 4 presents an experimental study on a complex structure, followed by conclusions in the final section.

2. Theoretical background

2.1. In-situ TPA

Consider an assembly of substructures A and B, coupled at the interface, as depicted in Fig. 1a. Substructure A is an active component with the operational excitation $\boldsymbol{f}_1$ acting at node 1. Meanwhile, no excitation force is acting on the passive substructure B. The responses on B in $\boldsymbol{u}_3$, $\boldsymbol{u}_4$, and also at the interface DoFs $\boldsymbol{u}_2$ are hence a consequence of the active force $\boldsymbol{f}_1$ only.

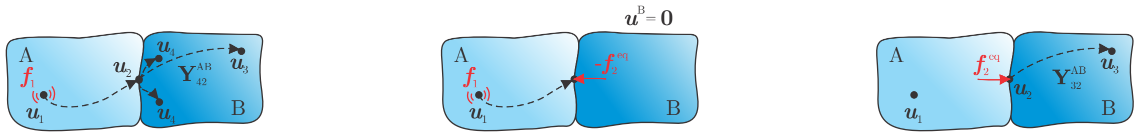

(a) (b) (c)

Figure 1: In-situ TPA: a) assembly of substructures A and B, b) $\boldsymbol{f}_2^{\mathrm{eq}}$ blocking the motion at the interface, c) replicating operational responses with $\boldsymbol{f}_2^{\mathrm{eq}}$.

Source excitations $\boldsymbol{f}_1$ are often not measurable in practice; therefore, in-situ TPA adopts a different approach for describing the operational excitations. A set of equivalent forces $\boldsymbol{f}_2^{\mathrm{eq}}$ is introduced, applied at the interface DoFs. If the source is deactivated, $\boldsymbol{f}_2^{\mathrm{eq}}$ yields the same responses on the passive side $\boldsymbol{u}_3$ as $\boldsymbol{f}_1$. The application of both the operational forces $\boldsymbol{f}_1$ and the equivalent forces $\boldsymbol{f}_2^{\mathrm{eq}}$ acting in the opposite direction simultaneously (Fig. 1b) should therefore remove any response on the passive side. The response at the interface $\boldsymbol{u}_2$ or at the indicator DoFs $\boldsymbol{u}_4$ can be used to calculate the equivalent forces, as follows[1]:

$$\mathbf{0} = \underbrace{\mathbf{Y}_{21}^{\mathrm{AB}}\boldsymbol{f}_1}_{\boldsymbol{u}_2} + \mathbf{Y}_{22}^{\mathrm{AB}}\left(-\boldsymbol{f}_2^{\mathrm{eq}}\right) = \underbrace{\mathbf{Y}_{41}^{\mathrm{AB}}\boldsymbol{f}_1}_{\boldsymbol{u}_4} + \mathbf{Y}_{42}^{\mathrm{AB}}\left(-\boldsymbol{f}_2^{\mathrm{eq}}\right). \tag{1}$$

Expressing the equivalent forces $\boldsymbol{f}_2^{\mathrm{eq}}$ from the indicator responses $\boldsymbol{u}_4$ yields:

$$\boldsymbol{f}_2^{\mathrm{eq}} = \left(\mathbf{Y}_{42}^{\mathrm{AB}}\right)^{+}\boldsymbol{u}_4. \tag{2}$$

The number of indicator responses $\boldsymbol{u}_4$ should exceed the number of $\boldsymbol{f}_2^{\mathrm{eq}}$, ensuring that the latter are properly observable from $\boldsymbol{u}_4$. Hence, the over-determined inverse problem is solved using a pseudo inverse, denoted

[1] An explicit dependency on the frequency is omitted to improve the readability of the notation, as will be the case for the remainder of the paper.

with the superscript $+$[2]. As seen from Eq. (1) a set of equivalent forces completely blocks all the interface motion and therefore the expression "blocked forces" can also be found in the literature [2].

Expressing $\boldsymbol{f}_2^{\text{eq}}$ in terms of both subsystem admittances using the Lagrange multipliers–FBS (LM–FBS) notation [1] means that an important observation can be made. The equivalent forces are a property of the active component only and are invariant with respect to any passive subsystem coupled to it. Therefore, they are transferable to an assembly with a modified passive side.

The responses at the passive side $\boldsymbol{u}_3$ are not considered in the determination of the equivalent forces (Eq. (1)). As such, they provide a useful tool to assess the completeness of the latter. The predicted response $\tilde{\boldsymbol{u}}_3$ as a consequence of $\boldsymbol{f}_2^{\text{eq}}$ only (Fig. 1c) can be expressed as:

$$\tilde{\boldsymbol{u}}_3 = \mathbf{Y}_{32}^{\text{AB}} \boldsymbol{f}_2^{\text{eq}}. \tag{3}$$

By comparing the predicted $\tilde{\boldsymbol{u}}_3$ and the measured $\boldsymbol{u}_3$ it is possible to evaluate whether the transfer paths through the interface are sufficiently well described by $\boldsymbol{f}_2^{\text{eq}}$. This approach can be useful for an on-board validation, when the prediction is performed on the assembly AB, or for a cross validation, when applied to the assembly with a modified passive side ($\text{A}\tilde{\text{B}}$).

2.2. Virtual point transformation

The theory of the VPT is summarized here according to [4, 6]. The main idea behind the VPT is to choose a virtual point near the physical interface of the substructure and obtain FRFs for n_{u} responses $\boldsymbol{u}$ and n_{f} excitations $\boldsymbol{f}$ in the proximity of this point ($\mathbf{Y}_{\text{uf}} \in \mathbb{C}^{n_{\text{u}} \times n_{\text{f}}}$). $\mathbf{Y}_{\text{uf}}$ is then projected onto the interface deformation modes (IDMs). If we assume only the rigid-body IDMs (rigid interface behaviour) then the virtual point has $m = 6$ DoFs, i.e., three translational and three rotational DoFs. In addition, flexible IDMs can also be considered to describe a more complex interface behaviour [22]. The transformation is achieved using the following equation:

$$\mathbf{Y}_{\text{qm}} = \mathbf{T}_{\text{u}} \mathbf{Y}_{\text{uf}} \mathbf{T}_{\text{f}}^{\text{T}}, \tag{4}$$

where $\mathbf{T}_{\text{u}}$ is the displacement transformation matrix and $\mathbf{T}_{\text{f}}$ is the force transformation matrix. $\mathbf{Y}_{\text{qm}} \in \mathbb{C}^{m \times m}$ is the VP FRF matrix with a perfectly collocated translation/rotation and force/moment DoFs. It is advisable that the number of measured responses and excitations, i.e., n_{u} and n_{f}, respectively, exceed the dimensions of the VP FRF matrix, $m \times m$ [4].

The kinematic relation between m responses at the virtual point $\boldsymbol{q}$ and n_u sensor displacements $\boldsymbol{u}$ can be written as:

$$\boldsymbol{u} = \mathbf{R}_{\text{u}} \boldsymbol{q}, \tag{5}$$

where $\boldsymbol{q}$ comprises three translations $\boldsymbol{q}_{\text{t}} = [q_X, q_Y, q_Z]^{\text{T}}$ and three rotations $\boldsymbol{q}_{\theta} = [q_{\theta_X}, q_{\theta_Y}, q_{\theta_Z}]^{\text{T}}$ of the VP. The IDMs are contained in $\mathbf{R}_{\text{u}} \in \mathbb{R}^{n_{\text{u}} \times m}$, which is a non-square matrix that provides the sensor locations and orientations with respect to the VP (Fig. 2). For more information about the assembly of the $\mathbf{R}_{\text{u}}$ the reader is referred to [6]. Solving Eq. (5) for $\boldsymbol{q}$ in a least-square sense yields the displacements of the VP:

$$\boldsymbol{q} = \left(\mathbf{R}_{\text{u}}^{\text{T}} \mathbf{R}_{\text{u}}\right)^{-1} \mathbf{R}_{\text{u}}^{\text{T}} \boldsymbol{u} = \mathbf{T}_{\text{u}} \boldsymbol{u} \quad \Rightarrow \quad \mathbf{T}_{\text{u}} = \left(\mathbf{R}_{\text{u}}^{\text{T}} \mathbf{R}_{\text{u}}\right)^{-1} \mathbf{R}_{\text{u}}^{\text{T}}. \tag{6}$$

Similarly, the loads $\boldsymbol{m}$ at the virtual point are obtained for a given vector of forces $\boldsymbol{f}$ in the proximity of the VP. Assuming rigid IDMs, $\boldsymbol{m}$ consists of three forces and three moments ($\boldsymbol{m} = [m_X, m_Y, m_Z, m_{\theta_X}, m_{\theta_Y}, m_{\theta_Z}]^{\text{T}}$). The contribution from all the input forces can be combined and expressed as follows:

$$\mathbf{m} = \mathbf{R}_{\text{f}}^{\text{T}} \mathbf{f}, \tag{7}$$

[2] The pseudo inverse based on singular value decomposition offers some insight into the inverse problem as singular values can be attributed by how each displacement space (each left singular vector) is observable from $\boldsymbol{u}_4$. Different regularization techniques can be applied accordingly to prevent a solution belonging to the smallest singular values from building up noise in $\boldsymbol{f}_2^{\text{eq}}$ if necessary [10].

[3] The position vector from the VP to the center of the sensor is denoted by $\boldsymbol{r}^k$. The unit vector for each accelerometer axis is $\boldsymbol{e}_i^k$ and the response in each axis is denoted by u_i^k $(i \in (x, y, z))$. The position vector from VP to the force impact is $\boldsymbol{r}^h$, the impact direction is $\boldsymbol{e}^h$ and the impact magnitude is f^h.

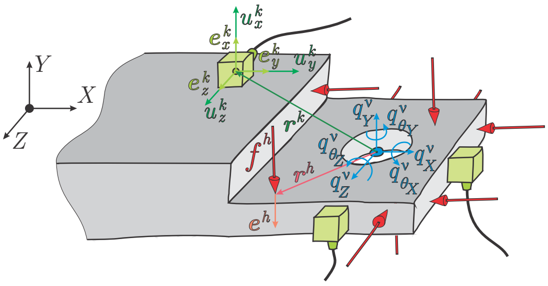

Figure 2: Projection of responses on the k-th triaxial accelerometer and the h-th excitation onto the virtual point[3].

where the IDM matrix $\mathbf{R}_\mathrm{f}^\mathrm{T} \in \mathbb{R}^{m \times n_\mathrm{f}}$ contains the positions and orientations for all the excitation locations with respect to the VP (Fig. 2). A more detailed description of $\mathbf{R}_\mathrm{f}$ is given in [6]. The inverse relationship of Eq. (7) is derived with a constrained minimization for forces:

$$\boldsymbol{f} = \mathbf{R}_\mathrm{f}\left(\mathbf{R}_\mathrm{f}^\mathrm{T}\mathbf{R}_\mathrm{f}\right)^{-1}\boldsymbol{m} = \mathbf{T}_\mathrm{f}^\mathrm{T}\boldsymbol{m} \quad \Rightarrow \quad \mathbf{T}_\mathrm{f}^\mathrm{T} = \mathbf{R}_\mathrm{f}\left(\mathbf{R}_\mathrm{f}^\mathrm{T}\mathbf{R}_\mathrm{f}\right)^{-1}. \tag{8}$$

For a more detailed explanation of the error minimization in the derivation of the transformation matrices $\mathbf{T}_\mathrm{u}$ and $\mathbf{T}_\mathrm{f}$ (including the use of the weighting matrix) the reader is referred to [4].

3. Characterization of random location errors in the TPA framework

To summarize, the determination of the equivalent forces using an in-situ approach requires the following measurements:

1. Measurement of the admittance matrix of the transfer paths $\mathbf{Y}_{42}^{\mathrm{AB}}$ (usually by impact or shaker testing on a non-operating system).

2. Measurement of the operational responses on the passive side $\boldsymbol{u}_4$ for a specific load case at the source.

In the following, the use of VPT in a $\mathbf{Y}_{42}^{\mathrm{AB}}$ measurement is assumed due to the advantages of including moments in the interface description [8] and non-rigid motion filtering at the low frequencies [23]. The VPT also filters the measurement errors to some extent by reduction of the forces in Eq. (7).

When obtaining $\mathbf{Y}_{42}^{\mathrm{AB}}$, impact testing is usually preferable to a shaker setup due to the practical FRF acquisition for each separate location. Therefore, the consistency of $\mathbf{Y}_{42}^{\mathrm{AB}}$ is strongly dependent on the hammer skills of the experimentalist, aiming to ensure good repeatability in the position between individual impacts. With the VPT, the impact locations should be in the proximity of the VP in order not to violate the assumption of the interface's rigidity. However, with a decreased distance the uncertainties associated with the position of the impacts are increased. Some insight into the location repeatability is available as the overall quality of the impact's transformation to the VP can be evaluated using measurement-quality indicators [4]. These indications compare the original (individual) with the filtered measurements (measurements transformed to the VP and then projected back to the initial location). However, a different approach to characterize the random location errors for the individual impact is adopted here.

Regarding the response measurements, accelerometers (or other response-measuring sensors) are mounted on the structure with a high degree of accuracy, as long as a proper fixation is ensured. Random location errors in the sensor placement can therefore be reduced with a carefully designed experiment and are not considered in the scope of this work.

3.1. Relation between the FRF and the impact location variation

The characterization of random location errors in structure excitation and their effect on the equivalent forces, presented here, is based on the findings of de Klerk and Visser [17, 18]. In general, the relationship describing the FRF and the impact location offset will be nonlinear. However, based on de Klerk [17], changes in the FRFs' real and imaginary parts due to the impact offset are linear in the proximity of the desired impact location. In the following, a simple numerical study is carried out on a structure depicted in Fig. 3, but only for the sake of demonstrating this relation.

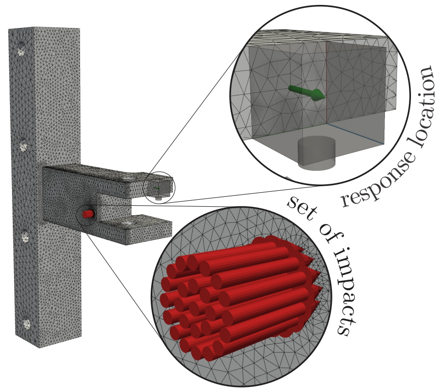

Figure 3: Demonstrative numerical model.

Numerical FRFs are generated for one excitation and one response location (zoomed in Fig. 3). At the excitation location, successive impacts are simulated, where each impact is subjected to the offset error within a circle in close proximity to the desired impact location[4]. Fig. 4 demonstrates that different FRFs are obtained for each impact. The anti-resonances change in frequency, while the amplitude of the resonances varies when the location errors are present.

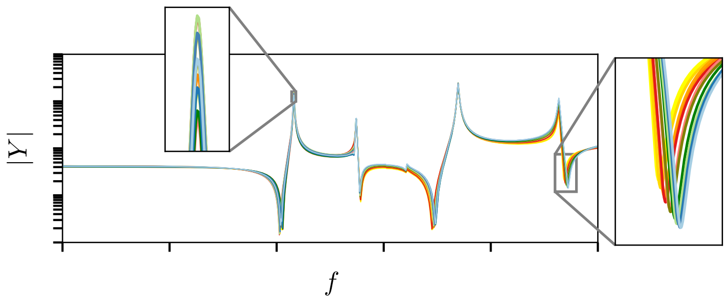

Figure 4: Effect of impact location offsets on the FRFs' magnitude. Axes values and labels are omitted because the purpose of the figure is only demonstrative.

Fig. 5 specifies the relationship between the calculated FRFs (treated as measured FRFs in the following) and the offset error. It is evident that the FRF entries in the complex plane form an elliptical shape for an individual frequency. The unidirectional variations for small location offsets are seen in the form of a linear dependency between the real and the imaginary parts, as was already established in [17]. Special care is given to the ellipse's major axis, as it corresponds to the direction for which the FRFs are the most sensitive to the errors in excitation location. Impacts spread in the direction most sensitive to the location errors therefore influence the measured admittance to the largest extent.

The equation for the ellipse's major axis can be formulated using an approximation approach. The

[4]Numerical FRFs of the structure are generated by means of the mode superposition method [4] based on first 100 eigenfrequencies and mass-normalised modes determined from the eigenvalue problem. Hence, the only variable in the FRF calculation is the impact position. A singular solution at the eigenfrequencies is avoided by defining the modal damping ratio.

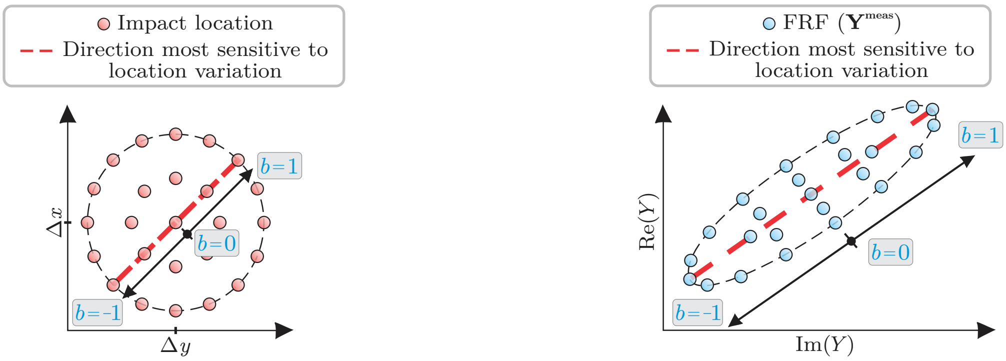

(a) (b)

Figure 5: Effect of impact location offsets on the FRFs for an individual frequency; a) idealized impact spread assuming circular boundary, b) set of FRFs with offset errors in the complex plane forming an elliptical shape with the ellipse's major axis orientated in the direction most sensitive to the location variation.

dependency of the real FRF part with respect to the relative impact location $\mathbf{b}$ is determined first:

$$\Re(\mathbf{Y}^{\text{meas}}) = k_{\text{r}}\,\mathbf{b} + n_{\text{r}}, \tag{9}$$

where:

$$\begin{aligned} k_{\text{r}} &= \frac{\max\left[\Re(\mathbf{Y}^{\text{meas}})\right] - \min\left[\Re(\mathbf{Y}^{\text{meas}})\right]}{2}, \\ n_{\text{r}} &= \frac{\max\left[\Re(\mathbf{Y}^{\text{meas}})\right] + \min\left[\Re(\mathbf{Y}^{\text{meas}})\right]}{2}. \end{aligned} \tag{10}$$

The values $\mathbf{b}$ are bounded by -1 and 1, where -1 corresponds to the minimum and 1 to the maximum real part. $\mathbf{Y}^{\text{meas}}$ consists of the measured FRFs with random location errors for multiple repetitions at a single excitation location. The dependency between the real and imaginary parts for the ellipse's major axis is obtained by approximating the ellipse in a complex plane with a linear relation:

$$\Im(\mathbf{Y}^{\text{meas}}) = k_{\text{i}}\,\Re(\mathbf{Y}^{\text{meas}}) + n_{\text{i}}. \tag{11}$$

In this manner, coefficients k_{i} and n_{i} are obtained. Based on Eqs. (9) and (11) the FRFs for multiple relative location errors in the most sensitive direction can be reconstructed:

$$\mathbf{Y}^{\text{rec}} = \Re(\mathbf{Y}^{\text{rec}}) + \mathrm{i}\,\Im(\mathbf{Y}^{\text{rec}}). \tag{12}$$

3.2. Global sensitivity analysis

If a sufficient number of samples is provided, the influence of an individual excitation location on the equivalent forces can be evaluated using a global SA. However, through the measurement process, it is practically impossible to obtain a sample size that is sufficient for SA. Therefore, the approach using Eq. (12) is adopted, where numerous FRFs can be reconstructed at each excitation location from a set of measured FRFs. In order to do so, the measured FRFs should not be averaged, but instead used to deduce the coefficients k_{r}, n_{r}, k_{i} and n_{i} (Eqs. (10) and (11)) at each frequency line as the most sensitive direction is also frequency dependent. For the reconstruction, a sizable set of relative impact locations should be provided. The Saltelli sample scheme[5] is proposed accordingly, where the number of input parameters is equal to the

[5]Saltelli sample scheme [19] is an extension of Sobol's sequence, a quasi-random low-discrepancy sequence used to generate uniform samples of parameter space. Using the Saltelli sample scheme, sensitivity indices are computed based on a reduced number of model evaluations. The Saltelli sample scheme is intended to be used later in Sobol's sensitivity analysis.

number of excitation locations. The obtained sample set presents small random offsets at impact locations and is bounded by the boundaries of $\mathbf{b}$, i.e., -1 and 1, respectively.

At an individual impact location, the FRFs are calculated for each sample (Eq. (12)). This is then repeated for all the excitation locations. The measured FRFs should not be added to the sample set as they do not coincide with the Saltelli sample scheme. Note that the reconstructed FRFs are generated only for locations that are positioned in the direction that is identified as being the most sensitive to the impact offset, as depicted in Fig. 6. Although the entire FRF spread is not included in the reconstruction process, the most dominant direction is considered sufficient to evaluate the effect of random location errors on the equivalent forces.

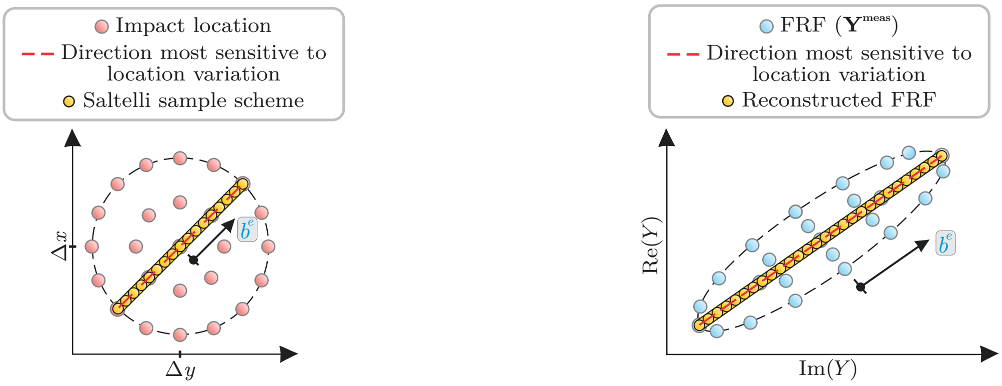

(a) (b)

Figure 6: Reconstruction of the FRFs in the most sensitive direction to the location variation following the Saltelli sample scheme: a) physical location of the positions for which FRFs are reconstructed, b) reconstructed real and imaginary parts of FRFs.

Each set of reconstructed FRFs from the Saltelli scheme is then used to estimate the equivalent forces. First, the VPT is applied to transform the forces onto the VP based on their relative position:

$$\mathbf{Y}_{\mathrm{um}} = \mathbf{Y}_{\mathrm{uf}}\mathbf{T}_{\mathrm{f}}^{\mathrm{T}}. \tag{13}$$

In this way, the admittances $\mathbf{Y}_{42}^{\mathrm{AB}}$ and $\mathbf{Y}_{32}^{\mathrm{AB}}$ are obtained. With the acquired operational response at the indicator sensors $\boldsymbol{u}_4$, Eq. (2) is then used to determine the equivalent forces for each sample set. Each set of forces is validated to assess how the validation varies due to the impact location variations. For this step, an on-board validation is considered the most appropriate[6]. The response $\tilde{\boldsymbol{u}}_3$ is predicted for each sample set using Eq. (3) and compared to the measured response $\boldsymbol{u}_3$. Various criteria can be applied to estimate the responses' agreement [8, 24]. In this study, the coherence criterion is used [8] as it is sensitive to both phase and amplitude differences.

Considering the on-board validation approach, the evaluation model for n excitation locations is equal to:

$$\begin{aligned}\chi_i(b_1^e, \dots, b_j^e, \dots, b_n^e) &= \frac{1}{N}\sum \operatorname{coh}(\tilde{u}_{3,i},\, u_{3,i}) = \\ &= \frac{1}{N}\sum \frac{(\tilde{u}_{3,i} + u_{3,i})(\tilde{u}_{3,i}^* + u_{3,i}^*)}{2(\tilde{u}_{3,i}^*\,\tilde{u}_{3,i} + u_{3,i}^*\,u_{3,i})} \quad \tilde{u}_{3,i} \in \tilde{\boldsymbol{u}}_3,\ u_{3,i} \in \boldsymbol{u}_3,\end{aligned} \tag{14}$$

[6]At this point, we are only interested in the variation of the equivalent forces due to the impact location variation. Hence, on-board validation is not used here to estimate the overall completeness of the transfer paths, but rather to provide a completeness criterion as a function of the impact location.

where the superscript $*$ denotes a complex conjugate. The variable χ_i is a scalar value of the averaged coherence over the full frequency bandwidth with N frequency points[7] and b_j^e is the e-th value of the impact offset from the Saltelli sample scheme for the j-th excitation location. The criterion is bounded between 0 and 1, with values closer to 1 indicating a strong correlation between the compared responses.

In order to quantify the influence of the random location error for an individual excitation on the $\boldsymbol{f}_2^{\mathrm{eq}}$, the use of Sobol's sensitivity analysis [20, 21] is proposed. The reason for using Sobol's SA is that it allows an estimation of the sensitivity indices for input parameters using only the output values of Eq. (14). The first-order Sobol's sensitivity index of each input parameter is defined as:

$$S_{1,j}^{\chi_i} = \frac{\mathbb{V}_{b_j}\left(\mathbb{E}_{\boldsymbol{b}_{\sim j}}[\chi_i|b_j]\right)}{\mathbb{V}(\chi_i)}, \tag{15}$$

where $\mathbb{V}(*)$ is the variance operator, $\mathbb{E}[*]$ is the expectation operator, b_j is the j-th input parameter (j-th impact) and $\boldsymbol{b}_{\sim j}$ is the set of all the parameters apart from b_j. The first-order index measures the main effect of the parameter b_j on the $\boldsymbol{f}_2^{\mathrm{eq}}$ alone. In other words, this is the contribution of the parameter b_j to the total variance $\mathbb{V}(\chi_i)$. For $\mathbb{E}_{\boldsymbol{b}_{\sim j}}[\chi_i|b_j]$ the mean of χ_i is taken over all possible values of $\boldsymbol{b}_{\sim j}$ while b_j is fixed [21]. The outer variance is then taken over all values of b_j. The parameter sensitivity is therefore estimated by how much the total variance is reduced for a fixed b_j. Dividing it by $\mathbb{V}(\chi_i)$ provides a fractional contribution to the total variance. The total order index measures the total effect of the parameter b_j, including the contribution of the variance due to the variable b_j alone, but also the contribution of any combination of b_j with the remaining input variables:

$$S_{\mathrm{T},j}^{\chi_i} = 1 - \frac{\mathbb{V}_{\boldsymbol{b}_{\sim j}}\left(\mathbb{E}_{b_j}[\chi_i|\boldsymbol{b}_{\sim j}]\right)}{\mathbb{V}(\chi_i)}. \tag{16}$$

Given that $\mathbb{V}_{\boldsymbol{b}_{\sim j}}\left(\mathbb{E}_{b_j}[\chi_i|\boldsymbol{b}_{\sim j}]\right)$ is the first-order effect of $\boldsymbol{b}_{\sim j}$, Eq. (16) gives the total effect of b_j [21].

3.3. *Quantification of impact sensitivity*

To summarize, the proposed approach to identify the excitation location with the highest influence on the equivalent forces is described briefly in the following steps:

STEP 1: Impact testing of the structure with at least two, but preferably up to ten, impacts per excitation location.

STEP 2: Deduction of the coefficients k_{r}, n_{r}, k_{i} and n_{i} for each element in the measured admittance matrix based on the FRF entries in the complex plane (Eqs. (10) and (11)) at each frequency.

STEP 3: Reconstruction of the FRFs for numerous variations in the impact location for the most sensitive direction (Eq. (12)). This is repeated for all the excitation locations. The Saltelli sequence should be used to generate the sample set for a number of input parameters equal to the number of excitation locations.

STEP 4: Calculation of the equivalent forces for each FRF set from the Saltelli scheme. First, the VPT is applied to transform the forces onto the VP. Then, Eq. (2) is used to determine the equivalent forces for each sample set.

STEP 5: On-board validation comparing the predicted response for each sample set $\tilde{\boldsymbol{u}}_3$ (Eq. (3)) and the measured response $\boldsymbol{u}_3$ using the coherence criterion (Eq. (14)).

STEP 6: Calculation of the first-order S_1 (Eq. (15)) and the total order S_{T} (Eq. (16)) Sobol sensitivity indices based on the on-board validation results.

[7] The coherence criterion and consequently the sensitivity analysis can also be validated for partial frequency bandwidths due to the dependence of the FRFs' spread on the frequency.

Based on the S_1 and S_T indices, one can determine how the variability of the individual impact location affects the estimated equivalent forces. High S_1 and S_T indicate that even a small deviation in the impact location can have a considerable effect on the on-board validation results. Hence, we propose to discard the excitation locations with standout sensitivity indices from the transfer path admittance. The source characterization should then be repeated using less location-sensitive impacts only. Care should be taken to retain a sufficient number of impacts in all directions and an over-determination of the VPT even after discarding the location-sensitive impacts.

Note that the direction that is most sensitive to variations in the impact location is also frequency dependent. Therefore, if we examine one FRF, reconstructed using the approximation approach, the impact associated with this FRF is in fact applied at different location at each frequency point. However, as Eq. (2) is also frequency dependent, this is not considered problematic for future calculations. The reconstructed FRFs are intended for the sensitivity analysis only. The use of reconstructed FRFs in the TPA characterization is discouraged and only measured FRFs should be used.

4. Experiment

To demonstrate the efficiency of the proposed approach, an experimental case study is presented next. A real complex structure, i.e., a brushless permanent magnet (BPM) motor, is fixed to a dedicated laboratory test bench. The transfer path admittance is obtained by impact testing. Firstly, the impacts that influence the equivalent forces in the strongest manner are identified using the Sobol sensitivity analysis. Secondly, the identified inconsistent impacts are removed from the source characterization, which is then evaluated via a comparison with the full impact set through on-board and cross validation. Both steps are performed for two different operational excitation cases: artificial excitation with an impulse hammer on the BPM motor housing and excitation from a constant rotation speed of the BPM motor.

4.1. Experimental setup

An assembly consisting of a BPM motor (active substructure) and a dedicated test-bench (passive substructure) is presented in Fig. 7. The electric motor is connected through four vibro-isolations to the

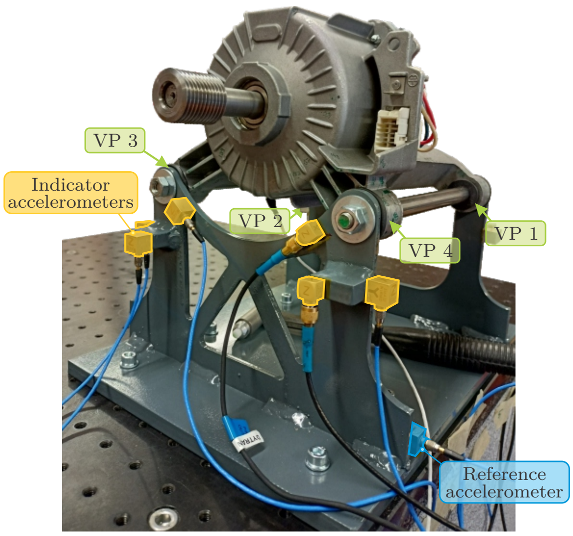

Figure 7: Test-bench with the BPM motor.

test-bench. The coupling points can be considered as point interfaces and the local rigidity required for the VPT can be assumed. The connectivity at the interface is ensured by two M8 threaded rods with a tightening torque of 5 Nm applied. Four transfer paths to characterize the equivalent forces between the substructures are considered. The frequency range of interest for the assembly lies between 0 Hz and 1200 Hz. A higher frequency range is omitted as the most influential harmonics of the electric motor in the application reach up to 1000 Hz when running.

Using the Python package *pyFBS* [25] the experimental setup is visualized in Fig. 8. The test-bench was equipped with 13 triaxial modal accelerometers PCB 356A32, where 12 of them (3 per transfer path) acted as indicators for the indirect determination of the equivalent forces and one as the target response. The accelerometers were positioned in the proximity of the interface to maximize the characterization quality [8, 9]. For the transfer path admittance measurement, impact testing was executed on a non-operating system. Twelve impacts per transfer path (virtual point) were chosen, placed in the proximity of the

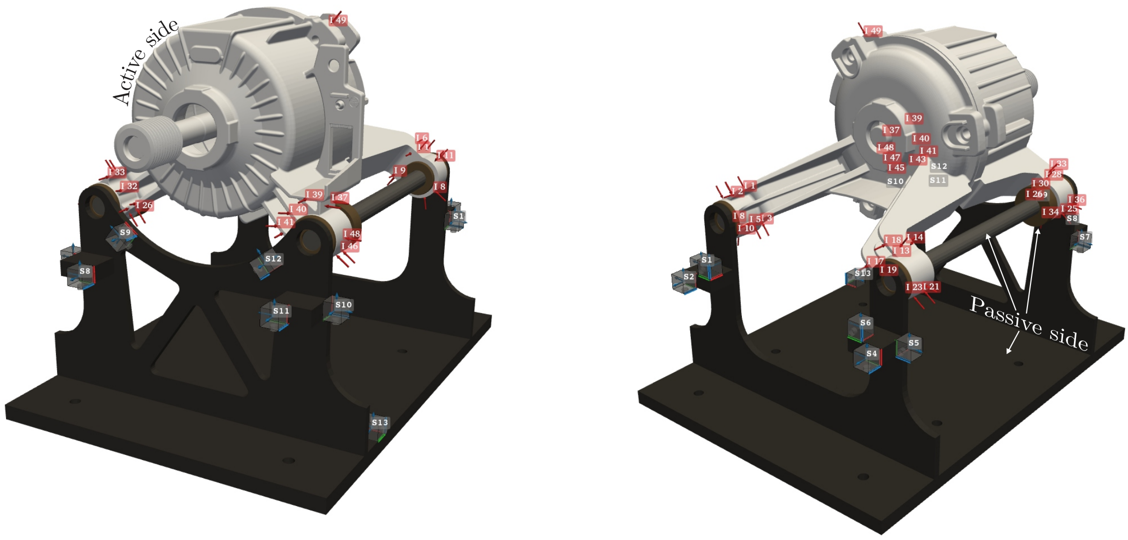

(a) (b)

Figure 8: Schematic presentation of the experimental setup: a) left view, b) right view. Darker colour scheme denotes the passive side (test-bench, connecting rods and vibro-isolations), while active side (electric motor) is depicted using bright colour.

interface on the active side in order not to violate the rigidity assumption. In this way, the vibro-isolations are regarded as a part of the passive substructure. The recommendations in [4] were considered when determining the impact locations[8]. The excitations were performed using the PCB 086C03 modal hammer with a vinyl tip. Eight impact repetitions were conducted per excitation location. Due to the complex geometry of the assembly, problems occur as some impact locations were not easily accessed with the impact hammer or were not visible from the experimentalist's point of view.

Fig. 9 demonstrates the effect of small random variations in the impact location on the measured FRF for one channel and one excitation. For eight impact repetitions, eight different FRFs are obtained. By plotting the measured FRFs in a complex plane (Figs. 10a and 10b) an elliptical shape is observed. On the ellipse's major axis, FRFs are then reconstructed for 512 samples from the Saltelli sample scheme and are displayed on Figs. 9 and 10.

4.2. Artificial operational excitation

When the assembly is subjected to the operating conditions of the BPM motor, only the main harmonics are dominant in the frequency spectrum. An additional impact location (I49), placed on the electric motor's housing was therefore used in the first experimental case as an artificial broadband source. In this way, the response of a passive substructure can be evaluated across the entire frequency range of interest. Due to

[8]Impacts were equally distributed in all directions and did not point straight to the VP in order to generate the moment load [4].

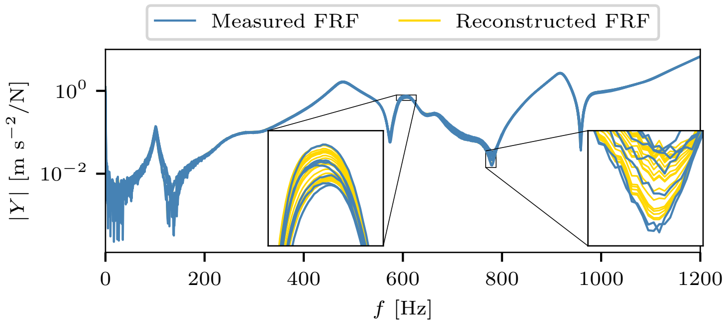

Figure 9: Experimentally obtained and reconstructed FRFs for the response at channel S1–y and the excitation at I1. For the sake of clarity, only every 20th reconstructed FRF is displayed.

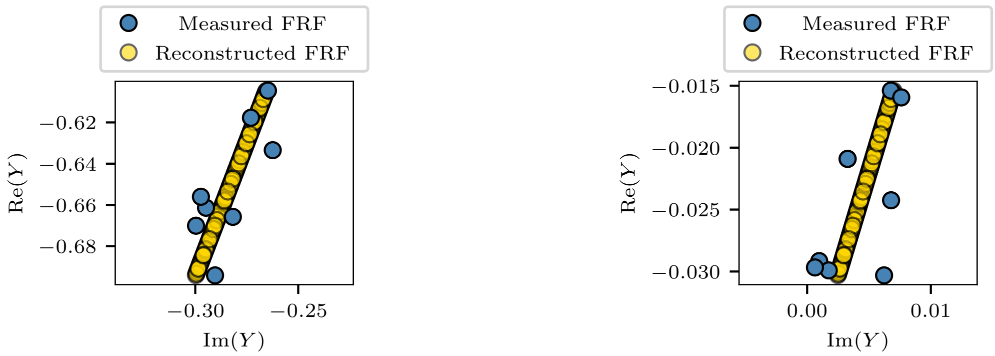

(a) (b)

Figure 10: Experimentally obtained and reconstructed FRFs for the response at channel S1–y and the excitation at I1 in the complex plane: a) at resonant frequency 602 Hz, b) at anti-resonant frequency 780 Hz.

the fact that higher responses at the sensors can be generated using an impact hammer, no regularization techniques were used for this test case, as the noise level is considered negligible.

Quantification of the impacts' sensitivity to location variation is performed according to the methodology given in Section 3.3. The results of the sensitivity analysis are presented in Fig. 11. The S_1 indices are averaged for all three predicted responses to comprise a random error characterization from all the references. It is more intuitive to characterize the location variations using only the first-order Sobol's sensitivity index, as it measures the main effect of the individual impact alone. Therefore, the total order index will be omitted from the rest of the paper.

Based on the S_1 indices, presented in Fig. 11, it is obvious that the equivalent forces are very sensitive to the location variations at the excitations I8, I23, I25, I34, I39 and I45. This is in agreement with the actual observations, as the listed impacts were challenging to reach and excite with an impact hammer. Hence, higher sensitivity indices for these locations were in fact expected. Based on Fig. 11, two different sets of impacts were determined: one set with all the impacts and one set with the consistent impacts only, where impacts with higher S_1 were omitted (Fig. 12). After the SA and for the source characterization, reconstructed FRFs were discarded. Instead, measured FRFs were used, which were averaged first in order to reduce the influence of the measurement noise. Using both sets, the impacts were first transformed to the virtual point (Eq. (13)). Then, the obtained admittance matrices $\mathbf{Y}_{42}^{\mathrm{AB}}$ were applied to determine the equivalent forces based on Eq. (2).

The consistency of the determined equivalent forces from both impact sets is evaluated next. First, an on-board validation (Eq. (3)) is performed where the consistent and all the sets of impacts are validated

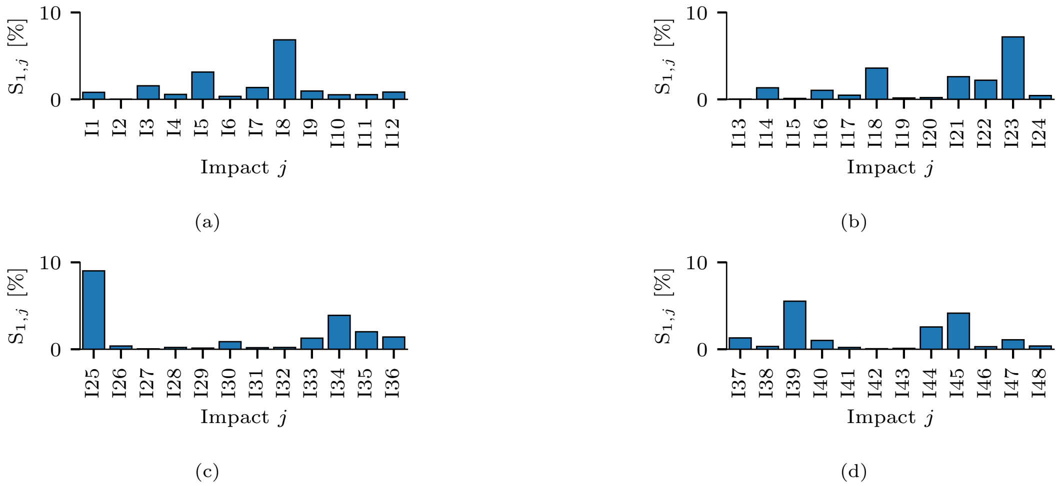

Figure 11: Averaged first-order Sobol's sensitivity indices for impacts at: a) 1st VP, b) 2nd VP, c) 3rd VP, d) 4th VP.

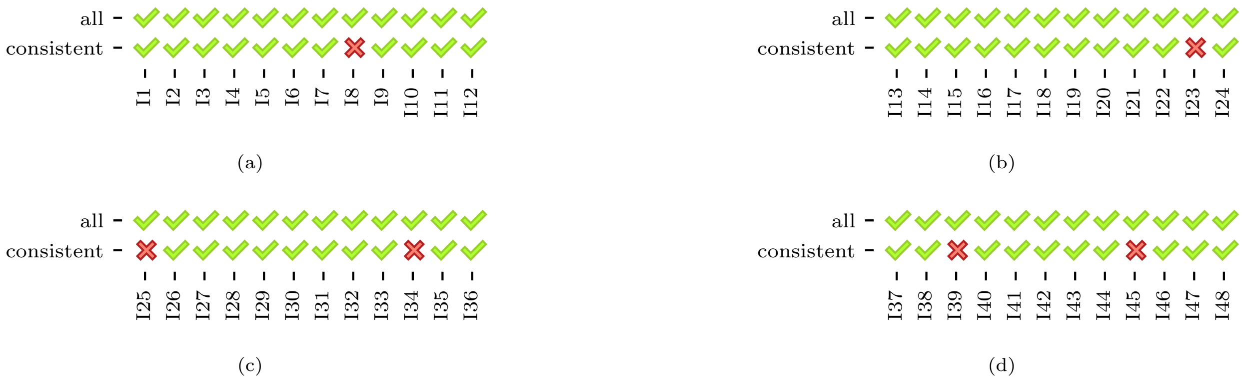

Figure 12: Set of impacts used for TPA characterization at: a) 1st VP, b) 2nd VP, c) 3rd VP, d) 4th VP. (✔) – Impacts retained in the VPT, (✖) – Impacts omitted in the VPT

on the original assembly AB. The sum of the transfer path contributions from individual equivalent forces yields a similar response prediction (Fig. 13). Both predictions match the reference with a high degree of accuracy, with minor improvements observed when a consistent set of impacts is considered for the source description.

Next, a cross validation is used, taking advantage of the equivalent forces being transferable to a new assembly with a modified passive substructure, $\mathrm{A}\widetilde{\mathrm{B}}$. The novel assembly is presented in Fig. 14. The BPM motor is mounted on the washing machine drum where the reference accelerometer is fixed. In order to replicate the operational excitation from the test-bench setup, the admittance $\mathbf{Y}^{\mathrm{A}\widetilde{\mathrm{B}}}_{3,\mathrm{I}49}$ is measured, where the structure is excited at an artificial source location (I49) and the response is captured with the reference accelerometer. Then, the impact signal from the test-bench setup is used to obtain the response $\boldsymbol{u}^{\mathrm{A}\widetilde{\mathrm{B}}}_3$, which is treated as a reference measurement.

In order to predict the response of the passive substructure based on both sets of determined equivalent forces, a measurement of the novel assembly's admittance $\mathbf{Y}^{\mathrm{A}\widetilde{\mathrm{B}}}_{32}$ is required[9]. Then, the responses $\tilde{\boldsymbol{u}}^{\mathrm{A}\widetilde{\mathrm{B}}}_3$ can

[9]Bias errors also manifest in the admittance matrix $\mathbf{Y}^{\mathrm{A}\widetilde{\mathrm{B}}}_{32}$. However, as this matrix is not inverted in Eq. (3), the bias errors in $\mathbf{Y}^{\mathrm{A}\widetilde{\mathrm{B}}}_{32}$ are considered negligible.

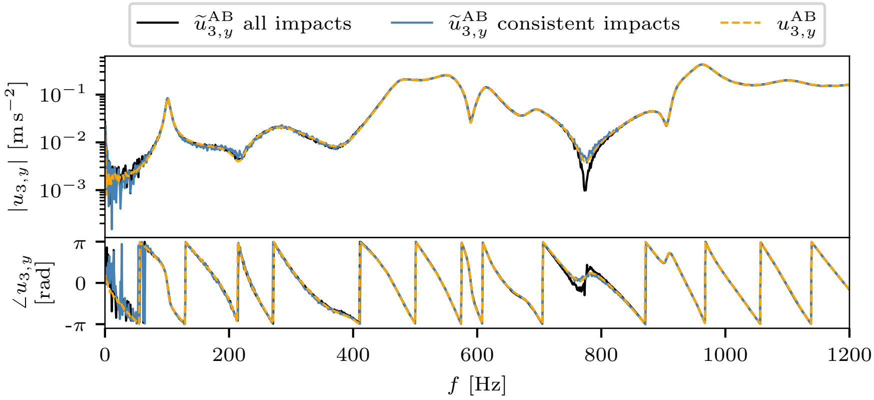

Figure 13: On-board validation of the determined equivalent forces based on all and the consistent sets of impacts using artificial impact excitation.

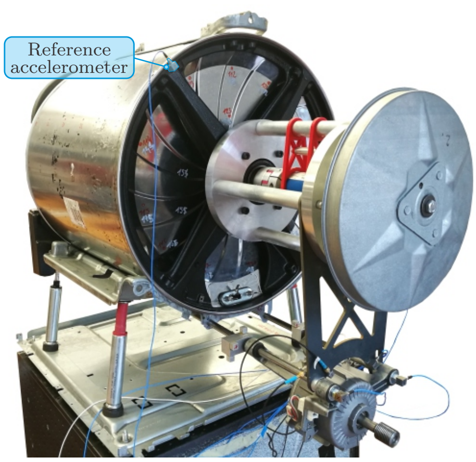

Figure 14: BPM mounted on the washing machine drum.

be predicted using:

$$\tilde{\boldsymbol{u}}_3^{\mathrm{A}\widetilde{\mathrm{B}}} = \mathbf{Y}_{32}^{\mathrm{A}\widetilde{\mathrm{B}}} \boldsymbol{f}_2^{\mathrm{eq}}. \tag{17}$$

Both $\tilde{\boldsymbol{u}}_3^{\mathrm{A}\widetilde{\mathrm{B}}}$, based on all and the consistent sets of impacts, respectively, are compared to the reference (Fig. 15). The magnitude and the phase of the responses are visualized. Both predicted responses match well with the reference. To some extent the measurement errors are already filtered by the VPT; however, a further improvement in the response prediction is observed when impacts with high sensitivity indices are removed from the source characterization. The response based on the identified consistent impacts is in better agreement with the reference for the majority of the frequency range of interest.

The correlation between the responses is additionally evaluated using the coherence criterion (Eq. (14)). The frequency-dependent criterion is evaluated for the entire frequency range and then averaged. The mean coherence values are presented in Fig. 16 for all three reference responses on the passive side. Excluding the impacts with higher S_1 leads to an improvement in the accuracy of the predicted response by 5%. With already established approaches (e.g., proper sensor positioning [9], implementation of the regularization techniques [9] and VPT [8] into TPA) a further improvement in the equivalent forces' completeness can be achieved using the proposed approach, even when dealing with highly damped structures.

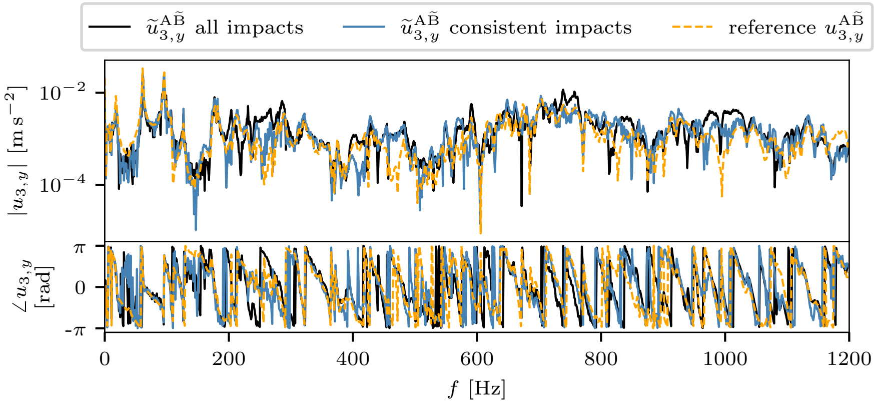

Figure 15: Cross validation of the determined equivalent forces based on all and the consistent sets of impacts using artificial impact excitation.

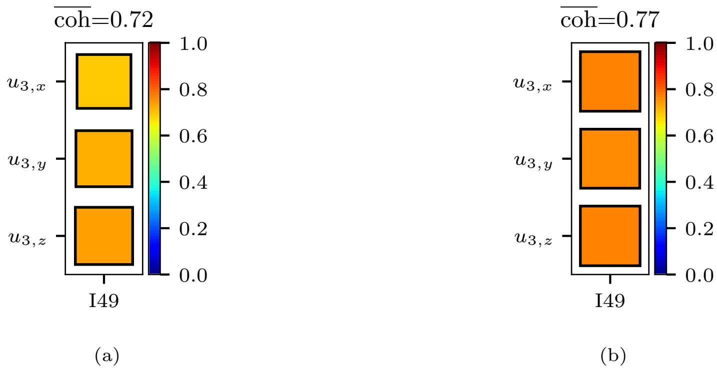

Figure 16: Cross validation of the determined equivalent forces based on: a) all impacts, b) consistent impacts.

4.3. Operational excitation

The second experimental case investigates whether the proposed approach is applicable to operational excitation where only the main harmonics are present in the frequency spectrum. The same test-bench setup is used as described in Section 4.1. The rotational velocity of the BPM motor was set to 336 Hz. The approach described in Section 3.3 was applied in order to identify impacts whose location variation influenced the determined equivalent forces to the greatest extent. For the SA, the coherence criterion was evaluated at frequencies only in the proximity of the electric motor's main harmonics. The calculation of the pseudo inverse in Eq. (2) was performed using the Tikhonov regularization [11]. The use of regularization techniques is advisable here to prevent the measurement noise from building up the equivalent forces due to the tonal excitation behaviour of the electric motor. If a pseudo inverse were to be computed using least squares, the noise on the indicator sensors would build up the equivalent forces as well as the true signal [9]. The regularization parameter α was determined using the Wiener filter [11], where the noise was recorded when the BPM was turned off. Using the SA, the sensitivities of the individual impacts based on 512 samples were obtained, as presented in Fig. 17.

Although the values of S_1 vary when compared to the first experimental case (Fig. 11) the same impacts can be recognized as location-sensitive. Note that the results of SA from Figs. 11 and 17 are not directly comparable due to the dissimilar examined frequency range for each experimental case. Again, impacts were divided into two sets, as presented in Fig. 12. The first set included all the impacts and the second set included only the consistent impacts. The equivalent forces were determined from both data sets and

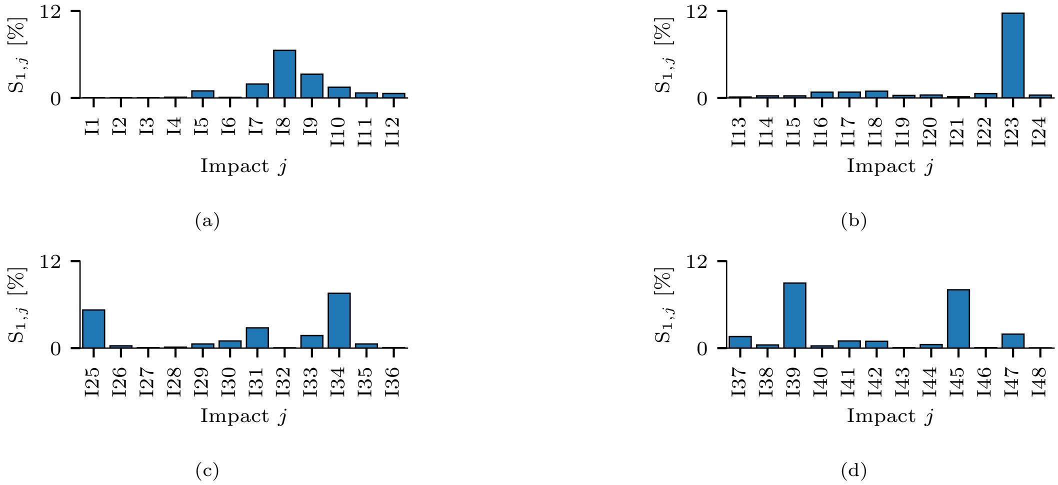

Figure 17: Averaged first order Sobol's sensitivity indices for impacts at: a) 1st VP, b) 2nd VP, c) 3rd VP, d) 4th VP. BPM motor was used for excitation in this experimental case.

then validated using cross validation on the modified structure A$\widetilde{\mathrm{B}}$. The predicted response $\tilde{\boldsymbol{u}}_3^{\mathrm{A}\widetilde{\mathrm{B}}}$ from both impact sets is compared with the measured response $\boldsymbol{u}_3^{\mathrm{A}\widetilde{\mathrm{B}}}$ in Fig. 18.

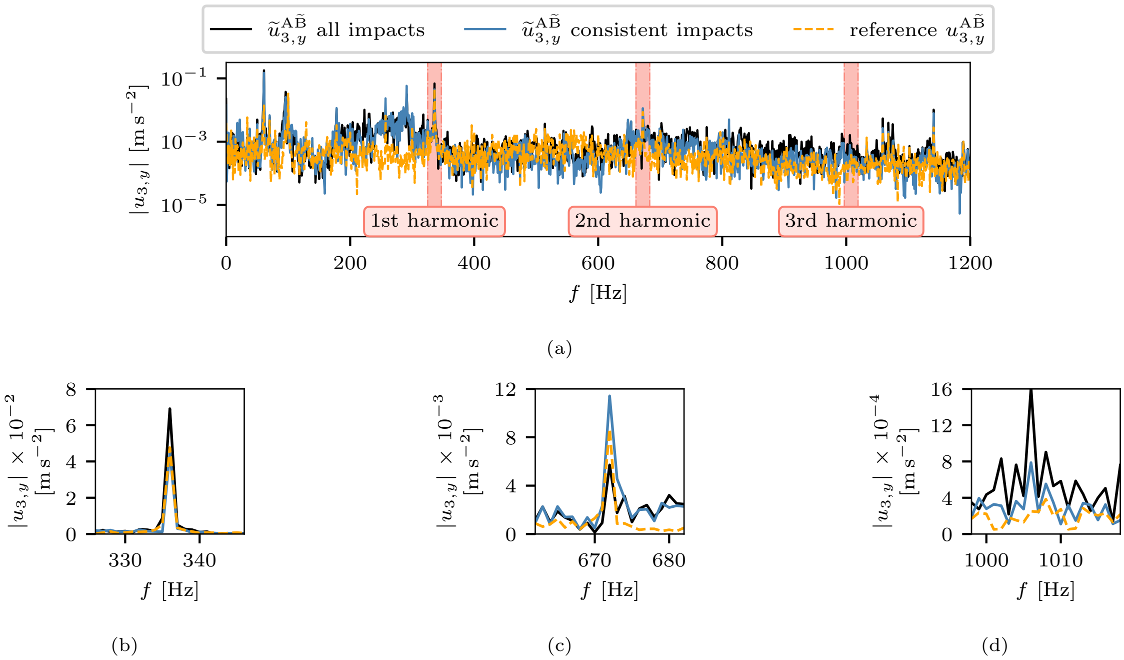

Figure 18: Cross-validation of the determined equivalent forces based on all and consistent set of impacts using operational excitation: a) response magnitude, b) 1st harmonic, c) 2nd harmonic, d) 3rd harmonic.

In the majority of the inspected frequency range, the measurement noise is dominant and any comparison is meaningless. The main harmonics of the BPM motor operating at 336 Hz are clearly visible in the frequency spectrum. Other dominant peaks appear due to the electrical interferences and at the natural frequencies of the assembly. A poor response prediction is observed between 200 Hz and 300 Hz for both sets of impacts. This is believed to be due an incomplete matrix regularization. By visually inspecting the predicted response with the reference at peaks above the noise floor, it can be observed that the prediction based on a set of consistent impacts matches the reference with a higher degree of accuracy. Magnifying the frequency regions at the main harmonics (Figs. 18b–18d) and plotting the response on a linear scale indicates that again a more consistent prediction is achieved using the set of impacts with low S_1.

The second experimental case demonstrates that the proposed approach is valid for operational excitation as well. No additional impact measurements are therefore needed. However, due to the presence of the main harmonics only and the majority of the response being below the noise floor, the criterion to reject inconsistent impacts must be carefully considered.

4.4. Discussion

Imprecise impact excitations are not the only error affecting the consistency of the equivalent forces. Transferability of the $\boldsymbol{f}_2^{\mathrm{eq}}$ based on either the consistent or all of the impacts is limited for this experimental case, as seen from Figs. 15 and 18. This is believed to be due to the two reasons: non-linear components of the assembly (e.g., vibro-isolations) behave differently for the operational condition compared to when the excitation is performed with an impact hammer to obtain the transfer path admittance. The second reason is the interface rigidity assumption. Higher in the frequency range a flexible interface motion is present, but filtered out from the VP loads, affecting the consistency of $\mathbf{Y}_{32}^{\mathrm{A}\tilde{\mathrm{B}}}$.

Based on the visual inspection of the predicted responses only minor improvements are observed when comparing consistent with the set of all of impacts in the lower frequency range, where the test object behaves rigidly. This is especially apparent in the case of on-board validation, with the stiff test-bench as the passive side (Fig. 13). At lower frequencies, contributions from translational equivalent forces are sufficient to produce an accurate response prediction [8, 23]. However, in the higher frequency range for the washing machine drum assembly, where the rotational DoFs are more prominent, the sensitivity-based approach of excluding location-sensitive impacts from the VPT provides a more accurate response prediction. The reconstruction of virtual moments is sensitive to deviations in the position of the hammer impact [4]. Hence, with the insight into the impact quality based on calculated sensitivity indices, an estimation of the virtual loads proves to be more consistent. It can be concluded that the approach is beneficial for cases when the experimentalist is not able to estimate the quality of the impacts performed (e.g., when the impact locations are hard to reach or are not visible from the experimentalist point of view). Another strong point is that the SA can be performed directly on the measured data, with no need for additional reference measurements or numerical models.

5. Conclusions

In this work, a sensitivity analysis is used to characterize the random location errors in a TPA framework, specifically aimed at small variations in the impact excitation location. The approach is well suited to admittance-based TPA methods, where the transfer path admittance is obtained with impact testing. A linear relation between the FRF and the impact's offset location is adopted in order to provide a sufficient sample size for the SA. Impact locations where small position variations influence the determined equivalent forces to the greatest extent can be identified and excluded from the source characterization. In this way, the experimentalist is given an insight into the quality of the impact position's repeatability.

The approach is useful for cases when the source characterization is affected by a random variation of the impact location, e.g., lightly damped structures or complex structures where the impact locations are not easily accessed. Additionally, random location errors in the response/load-sensor positioning can also be evaluated if the sensors' positions varies between successive measurements. As such, a characterization for a direct load determination at the interface is also available.

The applicability of the proposed methodology is demonstrated with an experimental case study of the assembly of an electric motor and a dedicated laboratory test bench. The identified inconsistent impacts were challenging to reach and excite with an impact hammer, hence substantial positional errors at these locations are expected. Excluding these impacts from the source characterization improves the prediction of the passive substructure's response, when the equivalent forces are transferred to a modified assembly.

Acknowledgements

The authors acknowledge partial financial support from the core research funding P2-0263 and the applied research project L2-1837, both financed by ARRS, the Slovenian research agency.

References

[1] M. V. van der Seijs, D. de Klerk, D. J. Rixen, General framework for transfer path analysis: History, theory and classification of techniques, Mechanical Systems and Signal Processing 68 (2016) 217–244.

[2] J. W. Verheij, Multi-path sound transfer from resiliently mounted shipboard machinery: Experimental methods for analyzing and improving noise control, Ph.D. thesis, TU Delft, Delft University of Technology (1982).

[3] D. Lennström, M. Olsson, F. Wullens, A. Nykänen, Validation of the blocked force method for various boundary conditions for automotive source characterization, Applied Acoustics 102 (2016) 108–119.

[4] M. van der Seijs, Experimental dynamic substructuring: Analysis and design strategies for vehicle development, Ph.D. thesis, Delft University of Technology (2016).

[5] A. Moorhouse, A. Elliott, T. Evans, In situ measurement of the blocked force of structure-borne sound sources, Journal of Sound and Vibration 325 (4-5) (2009) 679–685.

[6] M. V. van der Seijs, D. D. van den Bosch, D. J. Rixen, D. de Klerk, An improved methodology for the virtual point transformation of measured frequency response functions in dynamic substructuring, in: 4th ECCOMAS Thematic Conference on Computational Methods in Structural Dynamics and Earthquake Engineering, no. 4, 2013.

[7] M. Haeussler, S. Klaassen, D. Rixen, Experimental twelve degree of freedom rubber isolator models for use in substructuring assemblies, Journal of Sound and Vibration 474 (2020) 115253.

[8] M. Haeussler, T. Mueller, E. Pasma, J. Freund, O. Westphal, T. Voehringer, Z. F. AG, Component tpa: benefit of including rotational degrees of freedom and over-determination, in: ISMA 2020-International Conference on Noise and Vibration Engineering, 2020, pp. 1135–1148.

[9] M. Wernsen, M. van der Seijs, D. de Klerk, An indicator sensor criterion for in-situ characterisation of source vibrations, in: Sensors and Instrumentation, Volume 5, Springer, 2017, pp. 55–69.

[10] M. Häußler, Modular sound & vibration engineering by substructuring, Ph.D. thesis, Universität München (2021).

[11] M. Haeussler, D. Kobus, D. Rixen, Parametric design optimization of e-compressor nvh using blocked forces and substructuring, Mechanical Systems and Signal Processing 150 (2021) 107217.

[12] J. Meggitt, A. Moorhouse, A. Elliott, A covariance based framework for the propagation of uncertainty through inverse problems with an application to force identification, Mechanical Systems and Signal Processing 124 (2019) 275–297.

[13] J. Meggitt, A. Moorhouse, K. Wienen, M. Sturm, A framework for the propagation of uncertainty in transfer path analysis, Journal of Sound and Vibration 483 (2020) 115425.

[14] M. V. van der Seijs, E. A. Pasma, D. de Klerk, D. J. Rixen, A robust transfer path analysis method for steering gear vibrations on a test bench, in: Proceedings of the International Conference on Noise and Vibration Engineering (ISMA), Leuven, Belgium, 2014.

[15] M. Kodrič, G. Čepon, M. Boltežar, Experimental framework for identifying inconsistent measurements in frequency-based substructuring, Mechanical Systems and Signal Processing 154 (2021) 107562.

[16] Z. Saeed, C. M. Firrone, T. M. Berruti, Joint identification through hybrid models improved by correlations, Journal of Sound and Vibration 494 (2021) 115889.

[17] D. De Klerk, How bias errors affect experimental dynamic substructuring, in: Structural Dynamics, Volume 3, Springer, 2011, pp. 1101–1112.

[18] D. De Klerk, R. Visser, Characterization of measurement errors in experimental frequency based substructuring, ISMA 2010 Including USD2010 (2010) 1881–90.

[19] A. Saltelli, Making best use of model evaluations to compute sensitivity indices, Computer physics communications 145 (2) (2002) 280–297.

[20] I. M. Sobol, Global sensitivity indices for nonlinear mathematical models and their Monte Carlo estimates, Mathematics and computers in simulation 55 (1-3) (2001) 271–280.

[21] A. Saltelli, P. Annoni, I. Azzini, F. Campolongo, M. Ratto, S. Tarantola, Variance based sensitivity analysis of model output. Design and estimator for the total sensitivity index, Computer physics communications 181 (2) (2010) 259–270.

[22] E. Pasma, M. van der Seijs, S. Klaassen, M. van der Kooij, Frequency based substructuring with the virtual point transformation, flexible interface modes and a transmission simulator, in: Dynamics of Coupled Structures, Volume 4, Springer, 2018, pp. 205–213.

[23] J. Harvie, D. de Klerk, Source characterization for automotive applications using innovative techniques, in: Dynamic Substructures, Volume 4, Springer, 2021, pp. 117–125.

[24] J. Meggitt, A. Moorhouse, On the completeness of interface descriptions and the consistency of blocked forces obtained in situ, Mechanical Systems and Signal Processing 145 (2020) 106850.

[25] T. Bregar, A. El Mahmoudi, M. Kodrič, D. Ocepek, F. Trainotti, M. Pogačar, M. Göldeli, G. Čepon, M. Boltežar, D. J. Rixen, pyfbs: A python package for frequency based substructuring, Journal of Open Source Software 7 (69) (2022) 3399.